Biophysical *Journal*
Article

Biophysical Society

Force by minus-end motors Dhc1 and Klp2 collapses the *S. pombe* spindle after laser ablation

Parsa Zareiesfandabadi[1,3] and Mary Williard Elting[1,2,*]
[1]Department of Physics, North Carolina State University, Raleigh, North Carolina and [2]Cluster for Quantitative and Computational Developmental Biology, North Carolina State University, Raleigh, North Carolina

ABSTRACT A microtubule-based machine called the mitotic spindle segregates chromosomes when eukaryotic cells divide. In the fission yeast *Schizosaccharomyces pombe*, which undergoes closed mitosis, the spindle forms a single bundle of microtubules inside the nucleus. During elongation, the spindle extends via antiparallel microtubule sliding by molecular motors. These extensile forces from the spindle are thought to resist compressive forces from the nucleus. We probe the mechanism and maintenance of this force balance via laser ablation of spindles at various stages of mitosis. We find that spindle pole bodies collapse toward each other after ablation, but spindle geometry is often rescued, allowing spindles to resume elongation. Although this basic behavior has been previously observed, many questions remain about the phenomenon's dynamics, mechanics, and molecular requirements. In this work, we find that previously hypothesized viscoelastic relaxation of the nucleus cannot explain spindle shortening in response to laser ablation. Instead, spindle collapse requires microtubule dynamics and is powered by the minus-end-directed motor proteins dynein Dhc1 and kinesin-14 Klp2, but it does not require the minus-end-directed kinesin Pkl1.

SIGNIFICANCE *Schizosaccharomyces pombe* serves as an important model organism for understanding cell division. Its structurally simple mitotic spindle is especially suited for mechanical perturbation. Since *S. pombe* undergoes a process of closed cell division, without breakdown of the nuclear envelope, force may be exerted between its nuclear envelope and spindle. Here, we mechanically sever spindles via laser ablation to probe this force balance. After ablation, *S. pombe* spindle fragments collapse toward each other. We find that, contrary to prior expectations, forces from the chromosomes and nuclear envelope are not responsible for this collapse. Instead, it is microtubule dependent and is powered at least in part by the minus-end-directed microtubule motor proteins dynein Dhc1 and kinesin-14 Klp2.

INTRODUCTION

The mitotic spindle, a microtubule-based cellular machine, is responsible for accurate chromosome segregation in eukaryotes. During mitosis, spindle microtubules attach to the chromosomes, align them, segregate them, and physically deliver them to the two new daughter cells, ensuring each one has exactly one copy of the genetic information of the cell encoded in the chromosomes. Accurate chromosomes segregation is an essential function for life. Mis-segregation leads to aneuploidy, a condition of extra or missing chromosomes, associated with developmental defects and cancer in multicellular organisms (1,2). The mitotic spindle machinery is highly conserved across eukaryotes, likely due to its critical function.

Schizosaccharomyces pombe is a eukaryotic model system that is well-established for probing the microtubule cytoskeleton, including the mitotic spindle (3,4). Its geometrically simple spindle structure, which comprises a single bundle of microtubules (5), also makes it ideal for mechanical perturbation. *S. pombe* undergoes closed mitosis, with its nuclear envelope remaining intact during chromosome segregation (6,7). The timing of mitosis is highly uniform from cell to cell and can be divided into three distinct phases defined by the spindle length and rate of elongation (8): phase one, which includes prophase and spindle formation; phase two, which includes metaphase and anaphase A, during which spindle length remains constant at $\sim 2.5\ \mu$m; and phase three, which includes anaphase B, during which the spindle extends at a constant rate, elongating the nucleus

Submitted May 20, 2021, and accepted for publication December 16, 2021.
*Correspondence: mary.elting@ncsu.edu
Editor: William Hancock.
https://doi.org/10.1016/j.bpj.2021.12.019

into a dumbbell shape before it ultimately divides into two daughter nuclei.

Mitotic spindles are built of microtubule filaments oriented to form a bipolar structure. During *S. pombe* mitosis, microtubule minus-ends are anchored at specialized microtubule-organizing centers called spindle pole bodies (SPBs), and microtubule plus ends extend from these SPBs into both the cytoplasm and nucleoplasm (7,9). The spindle microtubules remain entirely nuclear, anchored at the two SPBs that are embedded in the nuclear envelope throughout mitosis (10). The astral population of microtubules, meanwhile, are nuclear before anaphase but extend into the cytoplasm during anaphase (11). These cytoplasmic astral microtubules may help to orient the spindle inside the cell (12–15), although their role is not entirely clear, and spindles can orient properly without them (3,16,17). Three classes of microtubules form the main bundle of the mitotic spindle itself: those that interdigitate in the mid-zone between the SPBs, those that emanate from one SPB and terminate at the other, and those that end at the kinetochore (5). Together, these microtubules and their associated proteins form a bipolar structure that ensures robust and symmetric chromosome segregation.

During elongation, *S. pombe* spindles, like those of other eukaryotes, must balance extensile and compressive forces (18–21). Extensile forces are provided by plus-end-directed microtubule motors that slide microtubules apart, most notably Cut7 in *S. pombe* (22), with some contributions from other motors, crosslinkers, and centromeres (23,24). Compressive forces can be provided by minus-end-directed motors (25–28), the chromosomes themselves (29,30), or in the case of closed mitosis, by the nuclear envelope (31,32). Stabilization of the spindle by microtubule crosslinkers, which might oppose either compressive or extensile forces, is also important for *S. pombe* spindle assembly (21,33–35).

Previous work probed force balance in the *S. pombe* spindle via laser ablation, demonstrating that microtubules within the spindle (rather than astral microtubules exterior to the nucleus) generate the force of spindle elongation (13,14). Importantly, these previous studies found that, after laser ablation, severed spindle fragments responded by collapsing toward each other. That work suggested that the collapse might be caused by the viscoelastic relaxation of the nuclear envelope and other materials inside the nucleus such as chromosomes, which deform in response to the extensile forces of spindle elongation (13,14). However, this model has not yet been tested, nor has the molecular basis of the collapse response been found.

Although viscoelastic deformation is one possible explanation for the collapse of *S. pombe* spindles in response to laser ablation, there is also a potential role for active rather than passive compressive forces. A minus-end-directed microtubule motor, of which there are three in *S. pombe* (Dhc1, Klp2, and Pkl1 (25,36,37)) seems the most likely candidate for such force generation.

Although none of the minus-end-directed motors are required for *S. pombe* mitosis (25,36,37), they all do have mitotic functions. Pkl1 localizes to SPBs, helping ensure that microtubule minus-ends remain anchored there (24,38). A double deletion *cut7*Δ*pkl1*Δ rescues *cut7*Δ, which is lethal, suggesting that Pkl1 may provide inward force that balances extensile sliding by Cut7 (28,33,39). Somewhat puzzlingly, though, *pkl1*Δ results in modestly shorter spindles (37). In contrast, *klp2*Δ cannot rescue *cut7*Δ (27). However, Klp2 does seem to contribute some inward-directed force to offset extensile sliding by Cut7 (28), and *klp2*Δ causes longer spindles (37). Localization and/or expression levels may contribute to these functional differences between the two kinesins. In mitosis, Klp2 tends to localize to the entire spindle rather than the poles, but targeting it to poles helps it to more effectively rescue *pkl1*Δ (27). Additionally, Klp2 may play a more important role in meiosis, when it is more highly expressed than Pkl1 and also localizes more prominently to poles than it does during mitosis (40). Finally, in stark contrast to many higher eukaryotes, where dynein is essential for maintaining spindle force balance and spindle pole integrity (41,42), *S. pombe* Dhc1 plays a more minor role in supporting chromosome biorientation and bundling microtubules at the SPBs (43,44). In sum, due to their complex and partially overlapping roles, it is not altogether clear which of these motors might be most likely to power the collapse of ablated spindles.

Here, we probe the physical mechanism of the collapse of the *S. pombe* spindle in response to laser ablation. We show that viscoelastic deformation of the nucleus does not explain this phenomenon, and instead find a role for microtubule-based force generation. We find that Dhc1 is partially responsible for reconnecting the poles of ablated spindles and pulling them toward each other, and that Klp2, but not Pkl1, also contributes.

MATERIALS AND METHODS

Strains, cell culture, and treatment with small molecule inhibitors

Fission yeast *Schizosaccharomyces pombe* strains used in this study are listed in Table S1. We followed standard growth conditions and media for all fission yeast cultures (45). We grew all strains on YE5S agar plates at 25°C before starting liquid cultures. We grew liquid cultures at 25°C with shaking by a rotating drum. For imaging, we grew MWE16 and MWE23 in YE5S liquid media for 12–24 h, washed three times using EMM5S, and further grew for 6–18 h in EMM5S liquid media before imaging. We grew MWE2, MWE10, MWE25, MWE27, MWE29, and MWE35 in YE5S media for 12–24 h before imaging.

For treatment with methyl 2-benzimidazole carbamate (MBC; Sigma 45,368-250M), we washed the cell cultures twice with the same growth media at the appropriate concentration of MBC, prepared from a 20 mM stock solution in DMSO that was stored at −20°C. We added latrunculin A (LatA; EMD Millipore) directly to the cell culture from a stock solution of 20 mM in DMSO. For DMSO control data (Figs. 4 and 5), we washed the cells twice with DMSO control media, which we prepared by adding 5 μL

of DMSO to 2 mL of YE, to match the final concentrations of DMSO in the MBC media described above. We conducted laser ablation experiments within 2–4 min of drug or DMSO addition.

Live-cell spinning disk confocal fluorescent microscopy and laser ablation

We prepared a slide for imaging using a gelatin or agar pad on a microscope glass slide. We made gelatin pads by heating 125 mg of gelatin with 500 μL of EMM5S at 90°C for 5–10 min using a table-top dry heat bath. We made agar pads by melting YE + 1% agar in a microwave. In both cases, we pipetted a small amount onto a glass slide, topped it with a coverslip, and allowed it to cool. We then centrifuged 1 mL of culture at log phase (verified by measuring optical density) at 3000 RCF using a table-top centrifuge, decanted the supernatant, and resuspended the pellet in 20 μL of media. We placed 5 μL of resuspended culture on the agar or gelatin pad and covered it with a coverslip. Immediately before imaging, we sealed the coverslip using VALAP (1:1:1 Vaseline:lanolin:paraffin).

We performed live-cell spinning disk confocal imaging with laser ablation at room temperature of 22°C as previously described (46–49). Briefly, we performed GFP imaging on a Nikon Ti-E stand on an Andor Dragonfly spinning disk confocal fluorescence microscope; spinning disk dichroic Chroma ZT405/488/561/640rpc; 488-nm (50 mW) diode laser (75 ms–120 ms exposures) with Borealis attachment (Andor); emission filter Chroma ET525/50m; and an Andor iXon3 camera. We performed imaging with a 100×1.45 Ph3 Nikon objective and a 1.5x magnifier (built-in to the Dragonfly system). For imaging of mCherry, we used the same settings as above except for confocal excitation with 561-nm diode laser (Andor) and emission filter Chroma ET 500/50m. We collected frames every 1–3 s for the duration of imaging. We performed targeted laser ablation using an Andor Micropoint attachment to the above microscope with galvo-controlled steering to deliver 10- to 15-ns pulses at 20 Hz using a dye laser. We used two different laser dyes in these experiments with emission maxima at 625 nm in cells expressing GFP-Atb2p + Htap1-mCherry (MWE10) and 551 nm for all other strains (Andor). For software, we used Andor Fusion software to control acquisition and Andor IQ software to control the laser ablation system simultaneously.

Analysis

We used ImageJ to crop and adjust brightness and contrast in all images. We also used ImageJ to convert the cropped TIF files to AVI format for further analysis (see below). For brightness and contrast, we used linear adjustment and did not use interpolation or compression at any stage.

After the initial cropping and adjustment with ImageJ, we performed all further analyses using home-built python codes using the Jupyter notebook environment. Analysis code is available upon request. Our software loads in the cropped image stacks as AVI files. We then used our software to record the location of the distal (presumed spindle pole body) ends of the spindles by manual tracking. We calculated the end-to-end Cartesian distance over time between these two tracked ends. We averaged the end-to-end distance traces for cells of the same treatment condition to measure the dynamics of the collapse more precisely. To average traces acquired with 1 and 3 s intervals, we set the value of 3-s interval traces to be the same for 3 s. We calculated the mean trace by averaging points from each trace at that time point and calculated the mean ± SE of all traces for each time point, and used it as an estimate on the error of this mean trace. We found the parameters, such as amplitude and τ, by fitting an exponential to the mean curve using the *curve_fit*() function in python.

The control mean trace of $n = 177$ cells in Fig. 1 *E* comprises results from strains MWE2, MWE10, and MWE16 strains not treated with MBC or LatA. Stepwise dropoffs visible in Figs. 4, 5, 6, and 7 mean traces are caused by individual traces having different durations.

RESULTS

S. pombe spindles collapse inward after laser ablation

To probe the mechanical stability and force balance of the mitotic spindle, we ablated spindles of live *S. pombe* cells expressing GFP-Atb2p (α-tubulin) (Fig. 1 *A*). Consistent with previous reports (13,14), we found that after severing the spindle in half via laser ablation, the fragments rapidly collapse toward each other (Fig. 1 *B*). In most cases, the two spindle fragments collapsed directly toward each other along the spindle axis (Fig. 1 *B*, Video S1). We also occasionally observed that the fragments rotated within the nucleus as their poles moved toward each other (Fig. 1 *C*).

Although the collapse of *S. pombe* spindles in response to laser ablation has been observed (13,14), previous work did not characterize the physical or molecular mechanism underlying it. To do so, we first quantified the collapse's dynamics by tracking the end of each spindle fragment after ablation and calculating the distance between them (49). A typical example trace is shown in Fig. 1 *D*, where we observe a sharp decrease in the pole-to-pole distance that begins immediately after ablation and continues for the next ~ 30 s. By averaging the trajectories for $n = 177$ ablated spindles, we determined that the average change in pole-to-pole distance over time follows an exponential relaxation response, as shown in Fig. 1 *E*. This mean trace fits well to an exponential function with magnitude $A = 0.84 \pm 0.02$ μm and time constant $\tau = 0.25 \pm 0.01$ min (errors reported as standard deviations from the least-squares fit).

Previous work (13,14) hypothesized that the spindle collapse in response to ablation might be caused by the viscoelastic relaxation of the nuclear envelope or chromosomes after disruption of extensile force from spindle elongation. Indeed, an exponential relaxation in response to ablation like the one we observe (Fig. 1 *E*) is consistent with a passive viscoelastic response (50). However, it is less clear that such a passive nuclear relaxation model could explain the spindle's rotation within the nucleus, which we would not expect to be accompanied by an overall change in nuclear shape (Fig. 1 *C*). Thus, we set out to test more directly whether forces from either rearrangement of the chromosomes within the nucleus or the nuclear envelope could explain spindle collapse.

Passive viscoelastic relaxation of chromosomes does not cause the spindle's collapse

Cohesin ensures sister chromatid cohesion and resists the poleward forces that pull the sister chromatids apart

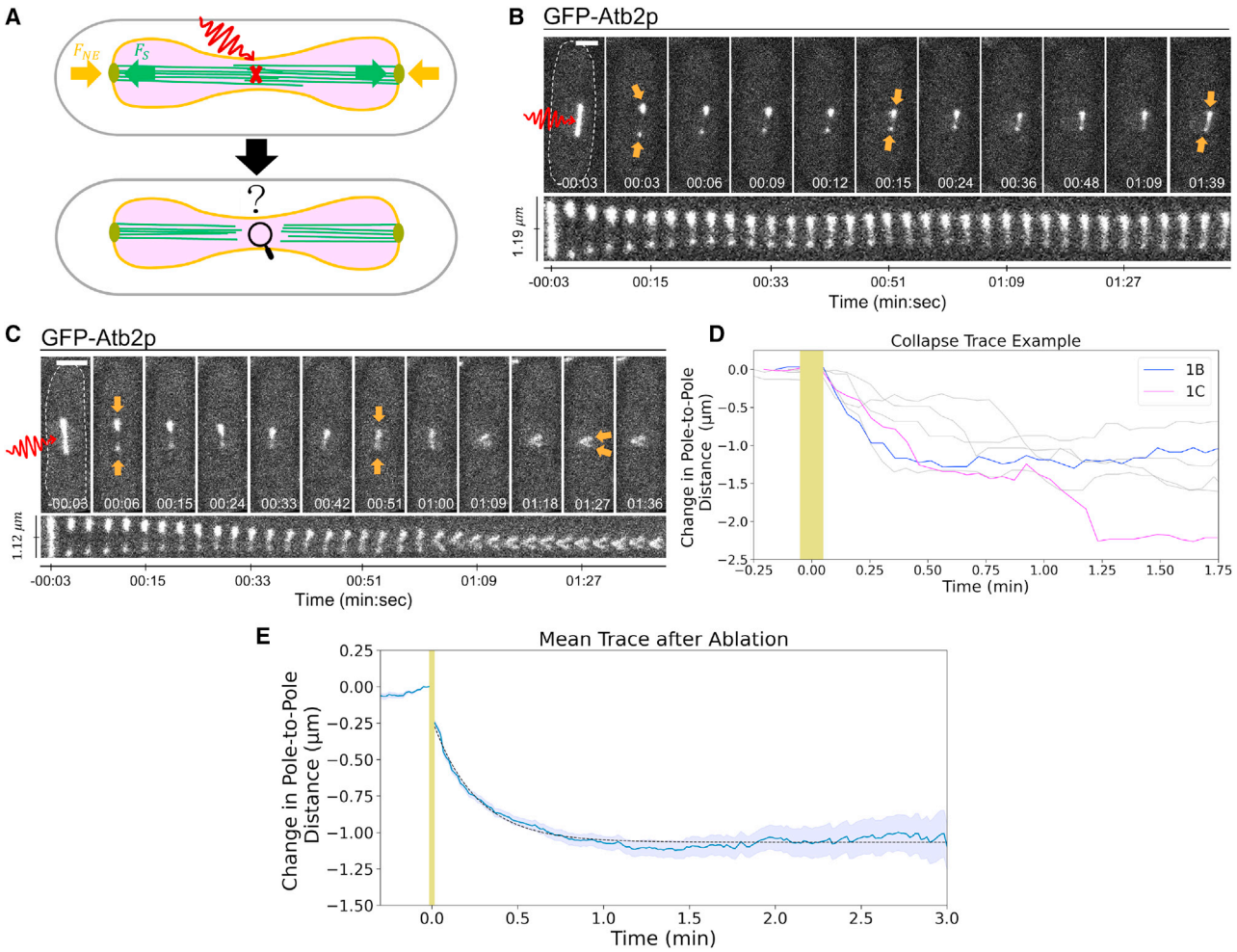

FIGURE 1 Response of the *S. pombe* mitotic spindle to laser ablation. (*A*) Experimental schematic. We target the spindle microtubules (green) in the *S. pombe* nucleus (magenta) for laser ablation (red X). We track the response of the spindle, the nuclear envelope (orange), and the spindle pole bodies (lime). Arrows indicate the presumed compressive force of the nuclear envelope, opposed by the extensile force of spindle elongation. (*B*) and (*C*) Two examples of *S. pombe* GFP-Atb2p spindles ablated near the mid-region during phase two of spindle elongation. Spindle ends (orange arrows) collapse toward each other after ablation (red). Top, highlighted frames; below, a montage of all frames. Dashed line in the first frame, cell boundary. Scale bars, 2 μm. Time, min:s. (*D*) Typical change in the pole-to-pole distance over time for several example spindles, including the one in B (blue) and in C (magenta). (*E*) The mean trace of change in pole-to-pole distance over time for $n = 177$ ablated spindles (solid blue line) and mean $\pm$ SE for all traces (blue shaded region). Black dotted line is a fit to an exponential, with amplitude 0.84 $\pm$ 0.02 μm and time constant 0.25 $\pm$ 0.01 min (errors, standard deviation on least squares fit). We cannot image during ablation, and the yellow shaded regions in (*D*) and (*E*) indicate this period.

(51,52), and entanglements between chromosomes, which will eventually be resolved by topoisomerases, resist sister chromatid separation as well (53,54). When anaphase begins, cohesin is gradually degraded, allowing the sisters to separate and move to opposite spindle poles (55). At the onset of stage three of spindle elongation, sufficient cohesin and entanglements between chromosomes may remain to allow the chromosomes to oppose spindle elongation (56). Budding yeast chromosomal DNA has been shown to act as an entropic spring (57), and *S. pombe* chromosomes likely have similar material properties. We would thus expect a roughly spherical equilibrium conformation for the chromosomes, and the nucleus as a whole. During spindle elongation, the chromosomes are stretched out of this equilibrium state by the growing spindle. We considered whether spindle collapse might be driven by a mechanical relaxation of the chromosomes themselves to a more spherical confirmation.

To test this hypothesis, we ablated the spindle in cells expressing GFP-Atb2p and Hta1p-mCherry (histone H2A-α) to observe the simultaneous response of chromosomes and the spindle to ablation (Fig. 2). If the relaxation of chromosomal DNA powers spindle collapse, we would expect to observe chromosomal rearrangements accompanying the spindle's movements.

However, after ablation, we could not detect any response of the histones in small spindles (before phase three of elongation). Although bleaching of the

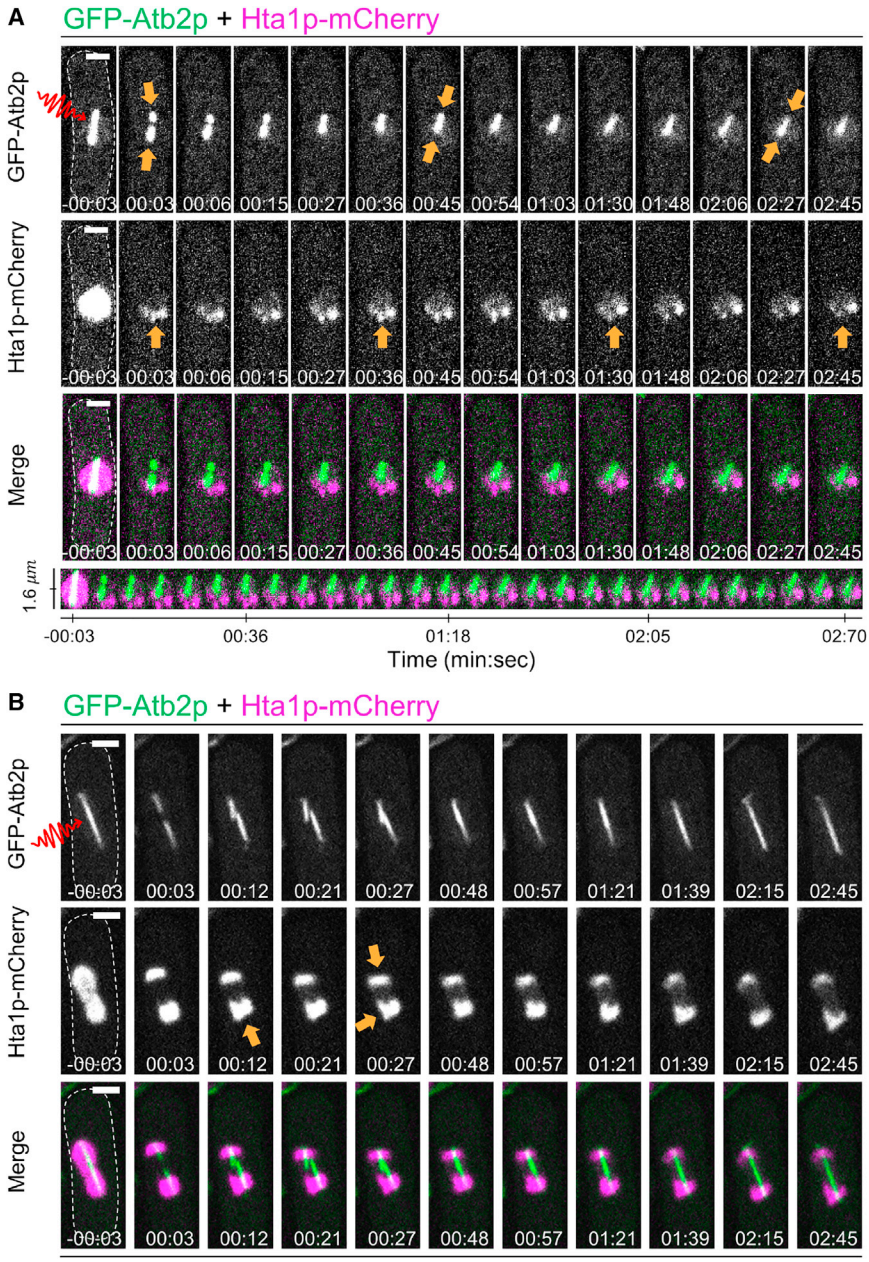

FIGURE 2 Response of histones to spindle laser ablation. (*A*) and (*B*) Two examples of *S. pombe* spindles expressing GFP-Atb2p plus Hta1p-mCherry and ablated near the mid-region during early phase three and mid-phase three of spindle elongation, respectively. Arrows point to spindle ends and histones, indicating the inward collapse of the spindle and histones' movement after ablation. A montage of collapse is displayed beneath for (*A*). The spindle collapses inward in both examples. Scale bars, 2 μm. Time, min:s.

Hta1p-mCherry signal by the ablation laser somewhat limits our observation immediately adjacent to the site of ablation, a detectable Hta1p-mCherry signal does remain after ablation (Fig. 2 *A* and *B*). This signal did not significantly change shape in small spindles as the spindle collapsed. In other words, the spindle movements we observed seemed to occur within a largely stationary nucleus (Fig. 2 *A*). The slight reorientation of the histones seen in Fig. 2 *A* is not correlated with the inward movement of the collapsing spindle. Although this observation is not wholly inconsistent with some chromosomal DNA movement, if significant rearrangement occurs, it must be very localized near the site of ablation (in the area that is bleached), and thus far from the translating SPBs.

In contrast, in longer spindles that had already entered phase three of spindle elongation before ablation, we did detect an inward histone movement that accompanied the collapsing spindle (Fig. 2 *B*). Interestingly, as the spindle collapsed, inward indentations near the ends of the spindle fragments appeared in the histone localization (see arrows in Fig. 2 *B*). This shape suggested inward pulling on the rest of the nucleus by the spindle during collapse rather than pushing on the spindle by the chromosomes. These spindle fragments then reconnected and resumed elongation.

Overall, these data do not support a strong role for viscoelastic relaxation of the chromosomes in underlying the collapse of either short or long ablated spindles. Therefore,

we next tested whether the nuclear envelope might be pushing spindle poles together after ablation.

Passive viscoelastic relaxation of the nuclear envelope does not cause the spindle's collapse

During spindle elongation, the *S. pombe* nucleus grows and deforms to accommodate the lengthening spindle (31,58,59). Pharmacological inhibition of fatty acid synthesis that prevents its growth can cause the nuclear envelope to exert sufficient force to bend or even break the spindle (31). Thus, it is clear that the nuclear envelope is capable of exerting compressive stress on the spindle. To test whether relaxation of the nuclear envelope back toward a spherical shape might have a role in spindle collapse, we repeated the ablation experiment with a strain that expresses both GFP-Atb2p to mark the spindle and nuclear envelope marker Cut11p-meGFP (58) (Fig. 3).

After ablation of small spindles, when the unperturbed nuclear envelope is not stretched and appears spherical, the collapsing spindle appeared to exert an inward pulling force on the nuclear envelope (Fig. 3 *A*, Video S2). This presumed inward force from the collapsing spindle induces a local inward curvature of the nuclear envelope. This shape change is not consistent with pushing from the nuclear envelope, so we conclude that the nuclear envelope does not power the collapse during stages one and two of mitosis, before the nucleus has begun to elongate.

We also considered whether the nuclear envelope might play a part in the collapse when the spindle has entered phase three of elongation and begun to increase the overall dimension of the nuclear envelope. If this were the case, we would expect the indentations shown in Fig. 3 *A* to be absent in longer spindles, and that longer spindles would have a correspondingly greater magnitude of collapse due to the larger tension forces in the nuclear envelope at this stage.

In contrast to this prediction, indentations near the poles are still present in the nuclear envelope of spindles ablated late in phase three (Fig. 3 *B* and *C*). Strikingly, in addition to indentations at the ends of spindle fragments, the nuclear envelope's surface became less smooth and symmetric in some of these nuclei (Fig. 3 *B*). Interestingly, in cells with a dumbbell-shaped nuclear envelope, the midsection's curvature remained after ablation (green arrows, Fig. 3 *B*).

We also examined whether the extent of spindle collapse correlated with the preablation spindle length. As illustrated in Fig. 3 *D*, we found that the minimum pole-to-pole distance strongly correlated with the precut spindle length (Spearman's correlation coefficient $= 0.830$). However, the extent of collapse, measured using change in pole length, exhibited only a very weak correlation (Spearman's correlation $= -0.144$). We interpret this to mean that spindles exhibit a similar degree of collapse irrespective of their length despite the presumed increase in envelope tension present in longer spindles.

In sum, we were unable to detect a role for nuclear envelope tension in spindle collapse at any stage of mitosis.

Actin is not a factor in the collapse of the spindle

After finding that passive nuclear relaxation could not explain spindle collapse, we next investigated the role of the cytoskeleton. Depolymerizing actin delays anaphase onset (60,61), likely by disrupting mitotic spindle stability (62), suggesting a possible role in spindle collapse. We examined whether actin was involved in spindle collapse by treating cells expressing both GFP-Atb2p and Cut11p-meGFP with latrunculin A (LatA) (Fig. 4). We ablated cells within 2–4 min after the addition of LatA, which depolymerizes actin filaments (Fig. S1).

As shown in Fig. 4 *A*, we observed a very similar collapse behavior in cells treated with 1 mM LatA as in untreated spindles. When we averaged the change in pole-to-pole distance over time for $n = 26$ spindles in cells treated with 1 mM LatA, we found that the magnitude and timescale of response were both very similar to control cells (Fig. 4 B). These data suggest that actin is not a factor in spindle collapse.

Microtubule dynamics are required for spindle collapse

We next tested whether the spindle itself might play an active force-generating role in spindle collapse. A rare observation shown in Fig. 5 *A* and Video S3 gave the first hint at a possible role for microtubules in the process. In this example, the spindle fragments first collapsed toward each other along the spindle's main axis and then rotated. While rotating, the spindle fragments at the ablation site remained connected as each fragments' end moved closer to the other. Shortly after, the GFP signal in the region between the ends increased (orange arrow, Fig. 5 *A*), and a new bundle of microtubules began to appear between the fragments. Although spindle fragments that reconnected outside the main spindle bundle were not often detectable, their observation in cases such as this one led us to investigate whether microtubules might be important for spindle collapse more generally.

To test whether spindle collapse was microtubule-dependent, we treated the cells with microtubule polymerization inhibitor methyl 2-benzimidazole carbamate (MBC) before ablation (Fig. 5 *B* and *C*, Video S4). At 100 μM MBC, few cells could maintain their spindles' integrity, and all small spindles were depolymerized. However, we were still able to visualize longer spindles, which were more resistant to depolymerization. We ablated these spindles and examined their response to ablation (Fig. 5 *B*). Spindle collapse was notably diminished in the presence of MBC. Instead of the

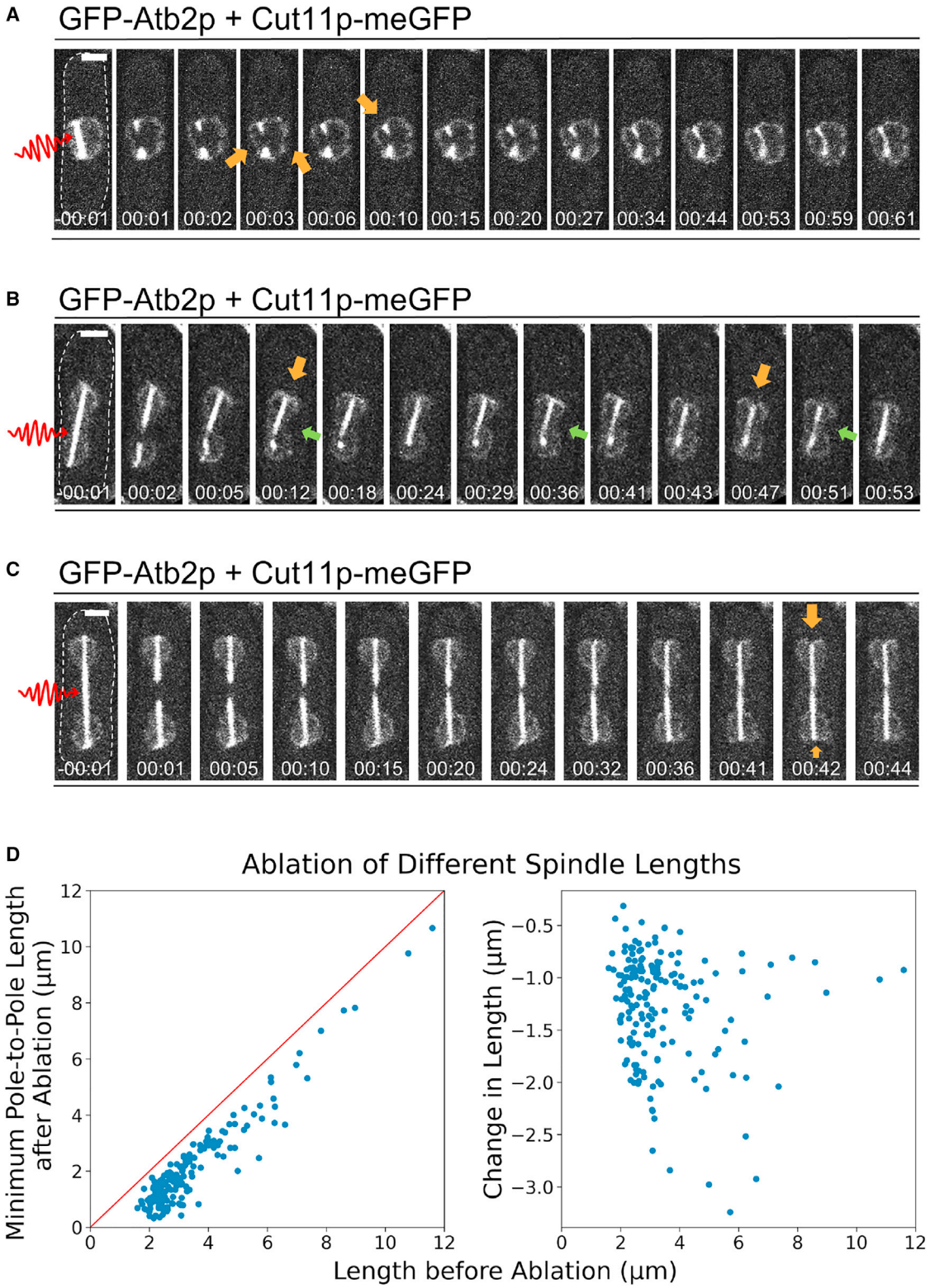

FIGURE 3 Pushing from the nuclear envelope on the spindle does not cause its collapse. (*A–C*) Three examples of *S. pombe* spindles expressing GFP-Atb2p and Cut11p-meGFP, ablated near the mid-region during phase two, mid-phase three, and late phase three of spindle elongation, respectively. Arrows mark the dents appearing at the nuclear envelope and cytoplasm boundary, indicating inward pulling forces after ablation. Scale bars, 2 μm. Time, min:s. Dashed line in the first frame illustrates the cell boundary for clarity. In all three examples, inward dents of the nuclear envelope appear at the ends of the spindles shortly after ablation (orange arrows). In (*B*), green arrows highlight that the nuclear envelope keeps its dumbbell shape after ablation. (*D*) Two scatter plots of $n = 177$ *S. pombe* control cells from Fig. 1 are shown. Left: scatter plot of minimum pole-to-pole length after ablation versus length before ablation, along with a linear function showing $y = x$ (red line). Right: scatter plot of collapsed length versus length before ablation.

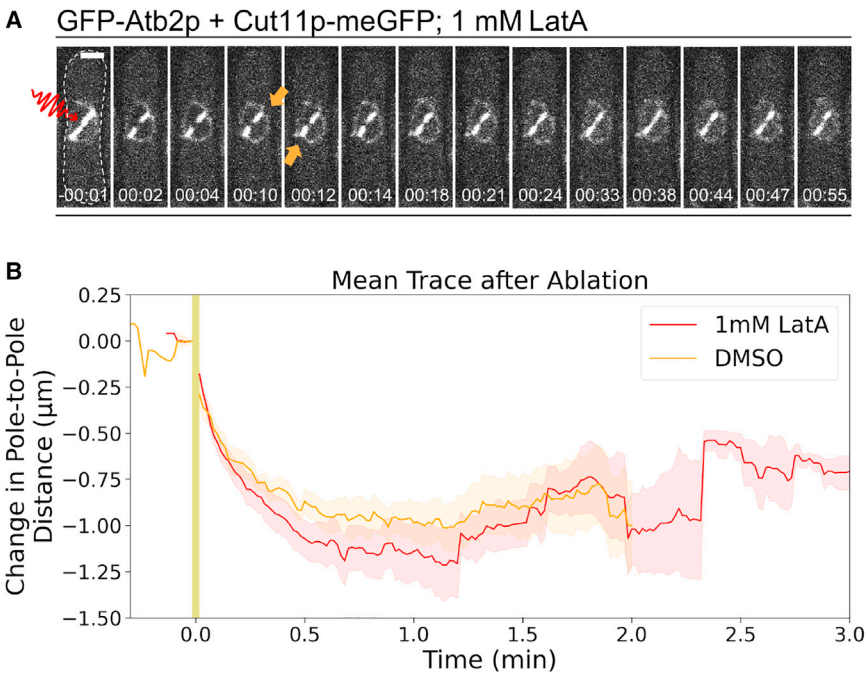

FIGURE 4 Actin depolymerization with latrunculin A does not affect spindle collapse. (*A*) Typical example of an ablated *S. pombe* spindle expressing GFP-Atb2p and Cut11p-meGFP treated with 1 mM latrunculin A during early phase three of spindle elongation. Arrows indicate nuclear envelope indentations after ablation. Dashed line in first frame indicates the cell membrane for clarity. Scale bar, 2 μm. Time, min:s. (*B*) The mean trace of change in pole-to-pole distance over time for $n = 26$ cells treated with 1 mM latrunculin A (red) is plotted along with a DMSO control ($n = 9$, orange). The shaded area shows the mean $\pm$ SE on each mean trace. We are unable to image during ablation, and the yellow shaded region indicates this period.

fragments collapsing toward each other, they appeared to be free to undergo rotational diffusion.

We also examined the response to spindle ablation at 25 μM and 50 μM MBC, where we were still able to find stage two spindles. Interestingly, we sometimes observed spindles at these concentrations that seemed to initiate collapse, with the spindle fragments reconnecting as the spindle length initially shortened, but then appeared to become detached again and undergo diffusion apart from each other (Fig. 5 *C*). Overall, collapse under this condition was lessened compared to untreated cells.

We quantified the pole-to-pole distance in ablated spindles at 25 μM, 50 μM, and 100 μM MBC (Fig. 5 *D*). In all cases, the mean spindle length does decrease over time, but it does so much more slowly and to a smaller extent than in control spindles, indicating that normal spindle collapse requires microtubule dynamics. However, we do not interpret this result to mean that spindle collapse is necessarily powered by microtubule dynamics *per se*. Instead, it is likely that when dynamics are perturbed, there is an overall lower availability of microtubules that can transduce inward force between SPBs. Similarly, the remaining collapse in the presence of MBC may still be microtubule-dependent, as we cannot completely inhibit microtubule dynamics without depolymerizing the spindle altogether.

Dhc1 contributes to the collapse of the spindle

The microtubule dependence of spindle collapse led us to hypothesize a role for a minus-end-directed microtubule motor, which might use microtubule tracks to pull the spindle fragments together and shorten the pole-to-pole distance. Dynein was an interesting candidate due to its known roles in maintaining spindle bipolarity and local force balance in higher eukaryotes (41,42,63,64). Although *S. pombe*'s sole dynein heavy chain, Dhc1, is required for normal meiosis but not mitosis (36), the evidence does suggest that it is involved in mitotic chromosome biorientation (43,44).

We examined the collapse response in *S. pombe* cells with dhc1 truncated after residue 1890 (65), which we refer to as *dhc1*ΔC. Spindle collapse was strikingly disrupted in *dhc1*ΔC cells (Fig. 6, Video S5). As with MBC treatment, the fragments of ablated spindles in *dhc1*ΔC cells often showed a prolonged diffusive search rather than a collapse (Fig. 6 *A* and *B*). On quantification, we found that the pole-to-pole distance in *dhc1*ΔC shows a much smaller decrease after ablation than control spindles (Fig. 6 *C*). Thus, dynein plays an important role in powering the collapse of the *S. pombe* spindle in response to ablation.

Minus-end-directed kinesin Klp2, but not Pkl1, contributes to the collapse of the spindle

Finally, we examined the role of the two *S. pombe* minus-end-directed kinesin motors, Klp2 and Pkl1. We found that spindles in cells with *klp2*Δ exhibited a smaller magnitude of collapse than control cells and that, similar to the effect seen in MBC and *dhc1*ΔC, the spindle fragments sometimes diffused more noticeably before collapse (Fig. 7 *A*). In contrast, *pkl1*Δ did not notably

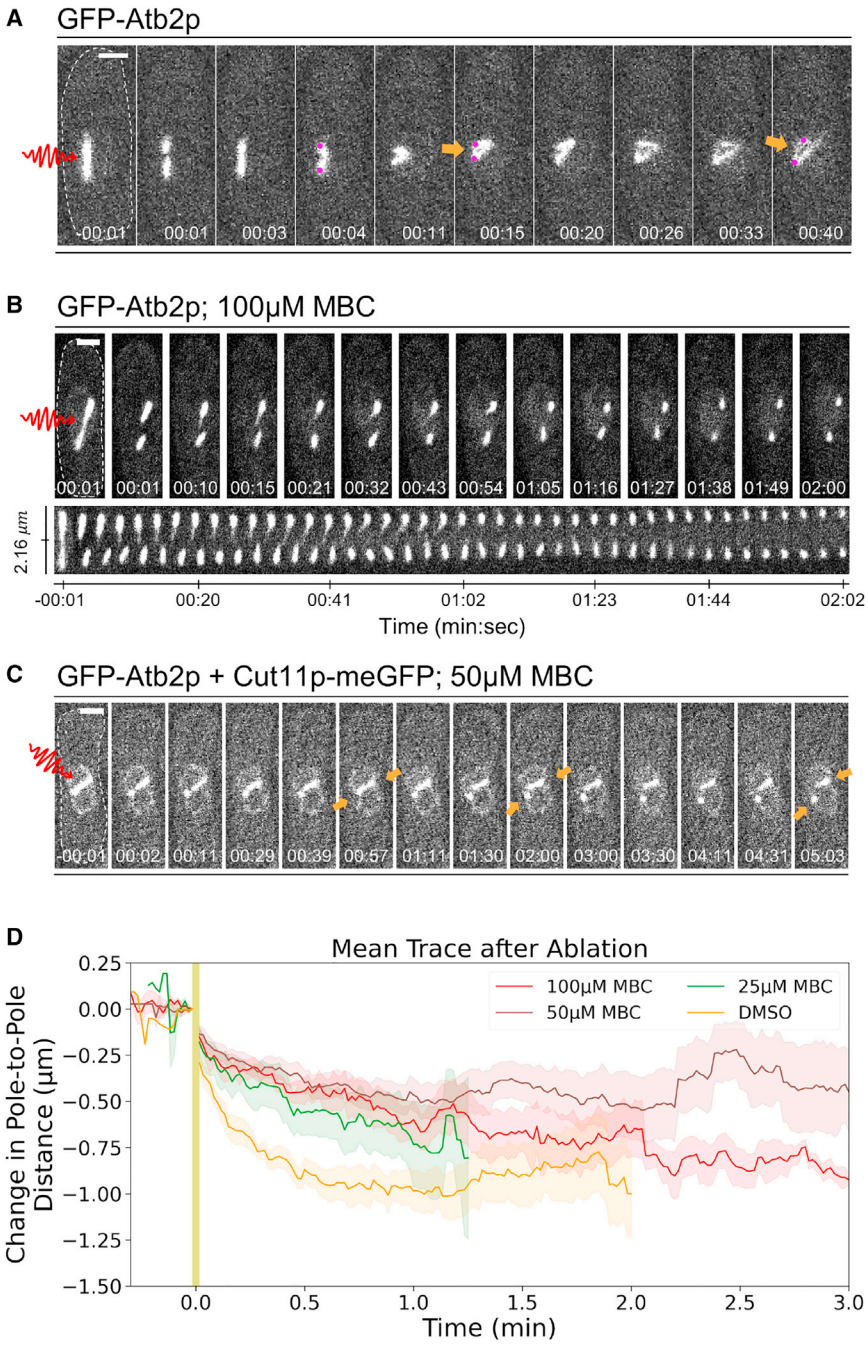

FIGURE 5 Spindle collapse after ablation requires microtubule dynamics. (*A*) Example *S. pombe* GFP-Atb2p spindle ablated near the mid-region during spindle elongation, showing connections of off-spindle-axis microtubules during its response. Arrows point to a bundle of microtubules. Circles (magenta) mark the supposed locations of spindle pole bodies. (*B*) Example *S. pombe* spindle ablation in a cell treated with 100 μM MBC, which does not lead to the spindle's collapse. A montage of the spindle after ablation is displayed beneath. (*C*) An example of *S. pombe* spindle expressing GFP-Atb2p plus Cut11p-meGFP spindle and ablated near one pole in a cell treated with 50 μM MBC during phase two of spindle elongation. The spindle collapses some but then seems to lose the connection between the poles. Arrows illustrate the changes in the nuclear envelope after ablation. Dashed line in the first frame illustrates the cell boundary for clarity. Scale bars, 2 μM. Time, min:s. (*D*) The mean trace of change in pole-to-pole distance over time for $n = 7$ cells treated with 100 μM MBC (red), $n = 23$ cells treated with 50 μM MBC (brown), and $n = 8$ cells treated with 25 μM MBC (green), is shown along with a DMSO control ($n = 9$, orange, same control as Fig. 4). The shaded area shows the mean $\pm$ SE on each mean trace. We are unable to image during ablation, and the yellow shaded region indicates this period.

affect spindle collapse (Fig. 7 *B*), and the double deletion of *klp2*Δ*pkl1*Δ behaved similarly to *klp2*Δ alone (Fig. 7 *C*). Quantification of poleward collapse supported these qualitative conclusions. Both *klp2*Δ and *klp2*Δ*pkl1*Δ spindles collapse to similar degrees as each other, whereas the collapse phase after ablation in *pkl1*Δ was indistinguishable from control (Fig. 7 *D*). The reduction for collapse in *klp2*Δ is similar although slightly smaller in magnitude to what we observed with *dhc1*Δ*C* (Figs. 6 *C* and 7 *D*), suggesting that both motors contribute to spindle collapse to a similar degree. Interestingly, we noticed that spindles in both *pkl1*Δ and *klp2*Δ seem to resume elongation more quickly than control spindles. Interrogating this behavior more closely will be an interesting area for future study.

DISCUSSION

Here, we have characterized the physical mechanism of the collapse of the *S. pombe* spindle in response to laser ablation. The two fragments of severed spindles collapse toward each other, and their end-to-end distance over

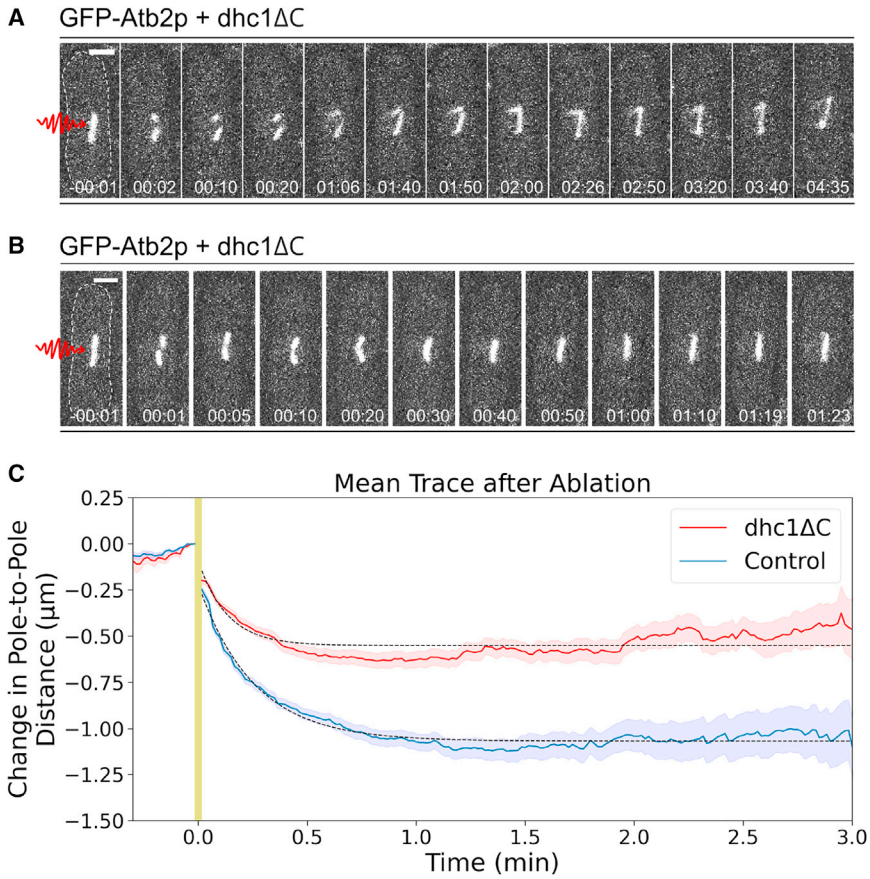

FIGURE 6 Spindles in *dhc1ΔC* cells exhibit reduced collapse after ablation. (*A* and *B*) Two example *S. pombe* GFP-Atb2p and *dhc1ΔC* spindles ablated near the mid-region during phase two of spindle elongation. Dashed line in the first frame illustrates the cell boundary for clarity. Scale bars, 2 μM. Time, min:s. (*C*) The mean trace of change in pole-to-pole distance over time for $n = 72$ ablated spindles in GFP-Atb2p plus *dhc1ΔC* cells is plotted (solid red line). Black dotted line is a fit to an exponential, with amplitude 0.45 ± 0.05 μM and time constant 0.13 ± 0.02 minute (errors, standard deviation on least squares fit). We also plot the analogous mean trace and exponential fit for $n = 177$ control untreated cells from Fig. 1 for comparison (blue). We are unable to image during ablation, and the yellow shaded region indicates this period.

time follows an exponential curve. The character of this response initially seemed consistent with viscoelastic relaxation, as was previously suggested (13,14). However, we find that neither the chromosomes nor the nuclear envelope respond in a way to suggest that they power the spindle collapse. If the envelope were producing the force needed for collapse, we would have expected the process to vary considerably with spindle length due to the significant changes in envelope shape over the course of mitosis. We do not observe such a dependence on spindle length. Instead, we observe nuclear envelope shape changes that appear to be generated by pulling forces generated from inside the nucleus. Although these data do not fully exclude the possibility that viscoelastic relaxation of the nucleus or nuclear envelope may contribute some inward force after collapse, they are not consistent with it as a primary driver. Actin depolymerization also does not affect the collapse.

Rather than the passive response that was previously predicted, we find that collapse is an active, microtubule-dependent process. C-terminal truncation of the minus-end-directed microtubule motor dynein Dhc1 disrupts spindle collapse, as does deletion of the minus-end-directed kinesin Klp2. We speculate that both motors may fulfill this function through minus-end-directed motor activity that carries spindle fragments as cargo after ablation. Although microtubule dynamics are required, their importance is likely important not for the dynamics themselves, but indirectly by increasing the availability of "tracks" that Dhc1 and Klp2 can walk along. We could not directly visualize these tracks, but we hypothesize that they are likely microtubules that remain anchored to the SPB and grow into the damaged area between the spindle fragments after ablation. Minus-end-directed motors could then carry the opposite spindle fragment toward the SPB, resulting in the collapse of the two SPBs toward each other. This mechanism would be similar to the role Klp2 is thought to play in recapturing "lost" kinetochores by walking them back to SPBs (66), but with spindle fragments rather than chromosomes as the cargo.

Although such poleward sliding and clustering of microtubule minus-ends has not been previously characterized for *S. pombe* Dhc1, dynein has been shown to play such a role in other organisms (67). For example, after laser ablation in mammalian cells, a complex of NuMA, dynein, and dynactin is enriched at new minus-ends and transports them poleward to re-anchor them to the spindle pole (63,64,68). Dynein is also critical for clustering minus-ends at spindle poles in many organisms (41,42,69). It may be that the simple geometry of the *S. pombe* spindle reduces its dependence on dynein-based clustering under normal conditions, but that the additional mechanical

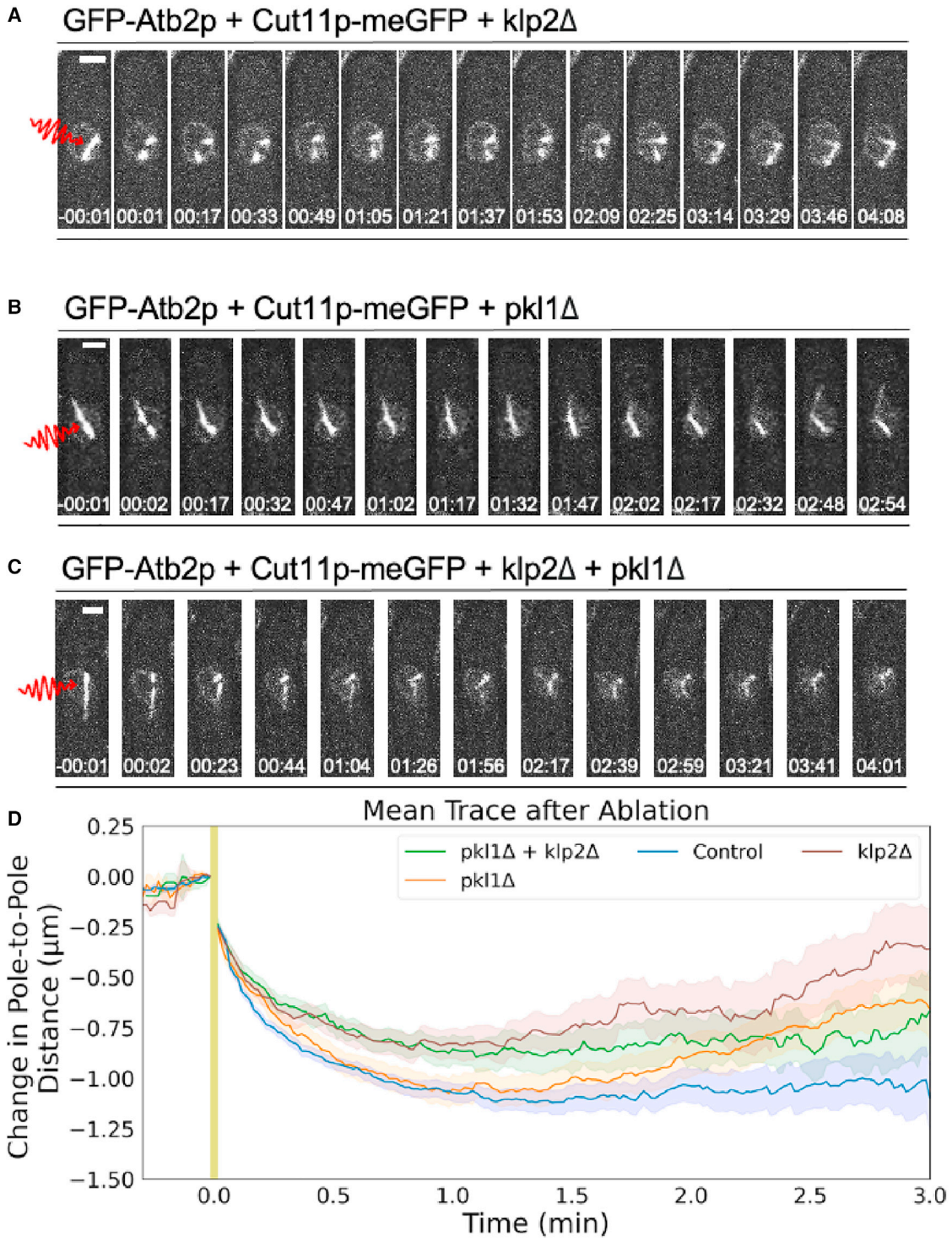

FIGURE 7 Spindles in *klp2*Δ but not *pkl1*Δ cells exhibit reduced collapse after ablation. Typical eample (*A*) *S. pombe* GFP-Atb2p, Cut11p-meGFP, and *klp2*Δ, (*B*) *S. pombe* GFP-Atb2p, Cut11p-meGFP, and *pkl1*Δ, and (*C*) *S. pombe* GFP-Atb2p, Cut11p-meGFP, and *klp2*Δ*pkl1*Δ spindles ablated near the mid-region during phase two of spindle elongation. Scale bars, 2 μM. Time, min:s. (*D*) The mean trace of change in pole-to-pole distance over time for ablated spindles with *klp2*Δ (brown, $n = 47$), *pkl1*Δ (orange, $n = 35$), and *klp2*Δ*pkl1*Δ (green, $n = 32$), compared with control spindles (blue, same data as Fig. 1 *E*). Shaded area shows the mean $\pm$ SE for each mean trace. We are unable to image during ablation, and the yellow shaded region indicates this period.

stress of laser ablation allows Dhc1 to step into a role similar to the more essential function its homologs play in other organisms.

It is interesting that Pkl1, despite its minus-end-directed motor activity, does not significantly contribute to the collapse of *S. pombe* spindles. One explanation for this

fact is that it localizes at mitosis primarily at SPBs (40), so it might not be properly localized to carry spindle fragments to SPBs as cargo. Another possible explanation is that its role as an antagonizer of microtubule nucleation (70) might offset a potential positive role in collapse as a cargo transporter.

A remaining question is how Dhc1 and Klp2 might localize and orient themselves to carry spindle fragments as minus-end-directed cargo. It is not yet clear whether the cell recognizes and recruits these complexes to damaged spindles, or whether motors that are already present on the spindle might fulfill this function. The known parallel bundling activity of Klp2 (26), as well as its localization throughout the length of the spindle (27), seem well suited to perform this function even without specific recognition of the damage due to ablation. In other higher eukaryotes, minus-ends of microtubules are specifically recognized to recruit dynein (63,64), but that recognition requires NuMA (68), which does not have a homolog in fission yeast. Thus, if similar recruitment is at work in *S. pombe*, it would require a different molecular mechanism.

In future work, it will be interesting to further examine the longer term response of the spindle as it resumes elongation after collapse. The differences in this behavior with *pkl*Δ and *klp2*Δ are notable and suggest a potential overall change in balance toward spindle elongation after ablation in these spindles. In addition, the behavior of the nuclear envelope in response to ablation raises important questions about its mechanics and how they are shaped by its physical connection to the spindle. For example, the preservation of a dumbbell-shaped envelope during spindle collapse suggests mechanical isolation of this region from the rest of the nuclear envelope, rather than a uniform surface tension distributed around the entire envelope. Laser ablation will be an important tool in addressing the cellular forces that underlie these shape changes.

SUPPORTING MATERIAL

Supporting material can be found online at https://doi.org/10.1016/j.bpj.2021.12.019.

AUTHOR CONTRIBUTIONS

P.Z. and M.W.E. designed experiments. P.Z. performed experiments and wrote analysis software. P.Z. and M.W.E. performed analysis and wrote the manuscript.

ACKNOWLEDGMENTS

We thank Eva Johannes and Mariusz Zareba of the NC State Cellular and Molecular Imaging Facility, Kerry Bloom, Arthur Molînes, Kimberly Bellingham-Johnstun, Gautam Dey, and members of the Elting lab for helpful discussions, and we thank Caroline Laplante, Fred Chang, Meredith Betterton, and J. Richard McIntosh for helpful discussions and for providing strains.

P.Z. acknowledges support by the Provost's Professional Experience Program, the Office of Undergraduate Research at North Carolina State University, and the National Society of Physics Students. M.W.E. acknowledges support by NIH R35GM138083 and NSF 1935260.

REFERENCES

1. Santaguida, S., and A. Amon. 2015. Short- and long-term effects of chromosome mis-segregation and aneuploidy. *Nat. Rev. Mol. Cell Biol.* 16:473–485.
2. Singh, V. P., and J. L. Gerton. 2015. Cohesin and human disease: lessons from mouse models. *Curr. Opin. Cell Biol.* 37:9–17. http://www.sciencedirect.com/science/article/pii/S0955067415001088.
3. Sawin, K. E., and P. T. Tran. 2006. Cytoplasmic microtubule organization in fission yeast. *Yeast.* 23:1001–1014.
4. Tolić-Nørrelykke, I. M. 2010. Force and length regulation in the microtubule cytoskeleton: lessons from fission yeast. *Curr. Opin. Cell Biol.* 22:21–28.
5. Ding, R., K. L. McDonald, and J. R. McIntosh. 1993. Three-dimensional reconstruction and analysis of mitotic spindles from the yeast, Schizosaccharomyces pombe. *J. Cell Biol.* 120:141–151. https://rupress.org/jcb/article/120/1/141/14563/Three-dimensional-reconstruction-and-analysis-of.
6. Mitchison, J. M. 1970. Chapter 7 physiological and cytological methods for Schizosaccharomyces pombe. *In* Methods in Cell Biology, *4*. D. M. Prescott, ed.. Academic Press, pp. 131–165.
7. Hagan, I. M., and J. S. Hyams. 1988. The use of cell division cycle mutants to investigate the control of microtubule distribution in the fission yeast Schizosaccharomyces pombe. *J. Cell Sci.* 89:343–357.
8. Nabeshima, K., T. Nakagawa, …, M. Yanagida. 1998. Dynamics of centromeres during metaphase – anaphase transition in fission yeast: dis1 is implicated in force balance in metaphase bipolar spindle. *Mol. Biol. Cell.* 9:3211–3225. https://www.molbiolcell.org/doi/10.1091/mbc.9.11.3211.
9. Sagolla, M. J., S. Uzawa, and W. Z. Cande. 2003. Individual microtubule dynamics contribute to the function of mitotic and cytoplasmic arrays in fission yeast. *J. Cell Sci.* 116:4891–4903.
10. McIntosh, J. R., and E. T. O'Toole. 1999. Life cycles of yeast spindle pole bodies: getting microtubules into a closed nucleus. *Biol. Cell.* 91:305–312. https://doi.org/10.1111/j.1768-322X.1999.tb01089.x.
11. Zimmerman, S., R. R. Daga, and F. Chang. 2004. Intra-nuclear microtubules and a mitotic spindle orientation checkpoint. *Nat. Cell Biol.* 6:1245–1246.
12. Oliferenko, S., and M. K. Balasubramanian. 2002. Astral microtubules monitor metaphase spindle alignment in fission yeast. *Nat. Cell Biol.* 4:816–820.
13. Tolić-Nørrelykke, I. M., L. Sacconi, …, F. S. Pavone. 2004. Positioning and elongation of the fission yeast spindle by microtubule-based pushing. *Curr. Biol.* 14:1181–1186. http://www.sciencedirect.com/science/article/pii/S0960982204004257.
14. Khodjakov, A., S. La Terra, and F. Chang. 2004. Laser microsurgery in fission yeast: role of the mitotic spindle midzone in anaphase B. *Curr. Biol.* 14:1330–1340. http://www.sciencedirect.com/science/article/pii/S096098220400510X.
15. Gachet, Y., S. Tournier, …, J. S. Hyams. 2004. Mechanism controlling perpendicular alignment of the spindle to the axis of cell division in fission yeast. *EMBO J.* 23:1289–1300.
16. Vogel, S. K., I. Raabe, …, I. Tolić-Nørrelykke. 2007. Interphase microtubules determine the initial alignment of the mitotic spindle. *Curr. Biol.* 17:438–444.
17. Daga, R. R., and P. Nurse. 2008. Interphase microtubule bundles use global cell shape to guide spindle alignment in fission yeast. *J. Cell Sci.* 121:1973–1980.

18. Blackwell, R., C. Edelmaier, …, M. D. Betterton. 2017. Physical determinants of bipolar mitotic spindle assembly and stability in fission yeast. *Sci. Adv.* 3:e1601603.

19. Elting, M. W., P. Suresh, and S. Dumont. 2018. The spindle: integrating architecture and mechanics across scales. *Trends Cell Biol.* 28:896–910.

20. Mogilner, A., and E. Craig. 2010. Towards a quantitative understanding of mitotic spindle assembly and mechanics. *J. Cell Sci.* 123:3435–3445.

21. Lamson, A. R., C. J. Edelmaier, …, M. D. Betterton. 2019. Theory of cytoskeletal reorganization during cross-linker-mediated mitotic spindle assembly. *Biophys. J.* 116:1719–1731.

22. Hagan, I., and M. Yanagida. 1990. Novel potential mitotic motor protein encoded by the fission yeast cut7+ gene. *Nature.* 347:563–566.

23. Shirasugi, Y., and M. Sato. 2019. Kinetochore-mediated outward force promotes spindle pole separation in fission yeast. *Mol. Biol. Cell.* 30:2802–2813.

24. Yukawa, M., C. Ikebe, and T. Toda. 2015. The Msd1–Wdr8–Pkl1 complex anchors microtubule minus ends to fission yeast spindle pole bodies. *J. Cell Biol.* 209:549–562.

25. Pidoux, A. L., M. LeDizet, and W. Z. Cande. 1996. Fission yeast pkl1 is a kinesin-related protein involved in mitotic spindle function. *Mol. Biol. Cell.* 7:1639–1655.

26. Braun, M., D. R. Drummond, …, A. D. McAinsh. 2009. The kinesin-14 Klp2 organizes microtubules into parallel bundles by an ATP-dependent sorting mechanism. *Nat. Cell Biol.* 11:724–730.

27. Yukawa, M., Y. Yamada, …, T. Toda. 2018. Two spatially distinct kinesin-14 proteins, Pkl1 and Klp2, generate collaborative inward forces against kinesin-5 Cut7 in S. pombe. *J. Cell Sci.* 131:jcs210740.

28. Yukawa, M., Y. Yamada, and T. Toda. 2019. Suppressor analysis uncovers that MAPs and microtubule dynamics balance with the Cut7/Kinesin-5 motor for mitotic spindle assembly in Schizosaccharomyces pombe. *G3 (Bethesda).* 9:269–280.

29. Bouck, D. C., A. P. Joglekar, and K. S. Bloom. 2008. Design features of a mitotic spindle: balancing tension and compression at a single microtubule kinetochore interface in budding yeast. *Annu. Rev. Genet.* 42:335–359.

30. Dinarina, A., C. Pugieux, …, F. Nédélec. 2009. Chromatin shapes the mitotic spindle. *Cell.* 138:502–513.

31. Yam, C., Y. He, …, S. Oliferenko. 2011. Divergent strategies for controlling the nuclear membrane satisfy geometric constraints during nuclear division. *Curr. Biol.* 21:1314–1319. http://www.sciencedirect.com/science/article/pii/S0960982211007251.

32. Takemoto, A., S. A. Kawashima, …, P. Nurse. 2016. Nuclear envelope expansion is crucial for proper chromosomal segregation during a closed mitosis. *J. Cell Sci.* 129:1250–1259.

33. Rincon, S. A., A. Lamson, …, P. T. Tran. 2017. Kinesin-5-independent mitotic spindle assembly requires the antiparallel microtubule crosslinker Ase1 in fission yeast. *Nat. Commun.* 8:1–12.

34. Yamashita, A., M. Sato, …, T. Toda. 2005. The roles of fission yeast ase1 in mitotic cell division, meiotic nuclear oscillation, and cytokinesis checkpoint signaling. *Mol. Biol. Cell.* 16:1378–1395.

35. Loïodice, I., J. Staub, …, P. T. Tran. 2005. Ase1p organizes antiparallel microtubule arrays during interphase and mitosis in fission yeast. *Mol. Biol. Cell.* 16:1756–1768.

36. Yamamoto, A., R. R. West, …, Y. Hiraoka. 1999. A cytoplasmic dynein heavy chain is required for oscillatory nuclear movement of meiotic prophase and efficient meiotic recombination in fission yeast. *J. Cell Biol.* 145:1233–1250. https://www.ncbi.nlm.nih.gov/pmc/articles/PMC2133150/.

37. Troxell, C. L., M. A. Sweezy, …, J. R. McIntosh. 2001. pkl1(+)and klp2(+): two kinesins of the Kar3 subfamily in fission yeast perform different functions in both mitosis and meiosis. *Mol. Biol. Cell.* 12:3476–3488.

38. Syrovatkina, V., and P. T. Tran. 2015. Loss of kinesin-14 results in aneuploidy via kinesin-5-dependent microtubule protrusions leading to chromosome cut. *Nat. Commun.* 6:7322.

39. Rodriguez, A. S., J. Batac, …, J. L. Paluh. 2008. Protein complexes at the microtubule organizing center regulate bipolar spindle assembly. *Cell Cycle.* 7:1246–1253.

40. Loncar, A., S. A. Rincon, …, P. T. Tran. 2020. Kinesin-14 family proteins and microtubule dynamics define S. pombe mitotic and meiotic spindle assembly, and elongation. *J. Cell Sci.* 133:jcs240234.

41. Verde, F., J. M. Berrez, …, E. Karsenti. 1991. Taxol-induced microtubule asters in mitotic extracts of Xenopus eggs: requirement for phosphorylated factors and cytoplasmic dynein. *J. Cell Biol.* 112:1177–1187.

42. Gordon, M. B., L. Howard, and D. A. Compton. 2001. Chromosome movement in mitosis requires microtubule anchorage at spindle poles. *J. Cell Biol.* 152:425–434.

43. Grishchuk, E. L., I. S. Spiridonov, and J. R. McIntosh. 2007. Mitotic chromosome biorientation in fission yeast is enhanced by dynein and a minus-end-directed, kinesin-like protein. *Mol. Biol. Cell.* 18:2216–2225.

44. Courtheoux, T., G. Gay, …, S. Tournier. 2007. Dynein participates in chromosome segregation in fission yeast. *Biol. Cell.* 99:627–637.

45. Forsburg, S. L., and N. Rhind. 2006. Basic methods for fission yeast. *Yeast.* 23:173–183. https://www.ncbi.nlm.nih.gov/pmc/articles/PMC5074380/.

46. Elting, M. W., M. Prakash, …, S. Dumont. 2017. Mapping load-bearing in the mammalian spindle reveals local kinetochore fiber anchorage that provides mechanical isolation and redundancy. *Curr. Biol.* 27:2112–2122.e5. http://www.sciencedirect.com/science/article/pii/S0960982217307200.

47. Begley, M. A., A. L. Solon, …, M. W. Elting. 2021. K-fiber bundles in the mitotic spindle are mechanically reinforced by Kif15. *Mol. Biol. Cell.* 32:br11.

48. Uzsoy, A. S. M., P. Zareiesfandabadi, …, M. W. Elting. 2021. Automated tracking of S. pombe spindle elongation dynamics. *J. Microsc.* https://doi.org/10.1111/jmi.13044.

49. Zareiesfandabadi, P., and M. W. Elting. 2021. Viscoelastic relaxation of the nuclear envelope does not cause the collapse of the spindle after ablation in S. pombe. *J. Undergrad. Rep. Phys.* 31:100013.

50. Roca-Cusachs, P., V. Conte, and X. Trepat. 2017. Quantifying forces in cell biology. *Nat. Cell Biol.* 19:742–751.

51. Bernard, P., J. F. Maure, …, R. C. Allshire. 2001. Requirement of heterochromatin for cohesion at centromeres. *Science.* 294:2539–2542.

52. Gerton, J. L. 2007. Enhancing togetherness: kinetochores and cohesion. *Genes Dev.* 21:238–241. http://www.genesdev.org/cgi/doi/10.1101/gad.1523107.

53. Piskadlo, E., and R. A. Oliveira. 2017. A topology-centric view on mitotic chromosome architecture. *Int. J. Mol. Sci.* 18:2751.

54. Kawamura, R., L. H. Pope, …, J. F. Marko. 2010. Mitotic chromosomes are constrained by topoisomerase II–sensitive DNA entanglements. *J. Cell Biol.* 188:653–663.

55. Tomonaga, T., K. Nagao, …, M. Yanagida. 2000. Characterization of fission yeast cohesin: essential anaphase proteolysis of Rad21 phosphorylated in the S phase. *Genes Dev.* 14:2757–2770.

56. Yukawa, M., Y. Teratani, and T. Toda. 2020. How essential kinesin-5 becomes non-essential in fission yeast: force balance and microtubule dynamics matter. *Cells.* 9:1154.

57. Vasquez, P. A., C. Hult, …, K. Bloom. 2016. Entropy gives rise to topologically associating domains. *Nucleic Acids Res.* 44:5540–5549.

58. West, R. R., E. V. Vaisberg, …, J. R. McIntosh. 1998. Cut11 +: A gene required for cell cycle-dependent spindle pole body anchoring in the nuclear envelope and bipolar spindle formation in Schizosaccharomyces pombe. *Mol. Biol. Cell.* 9:2839–2855.

59. Saitoh, S., K. Takahashi, …, M. Yanagida. 1996. Aberrant mitosis in fission yeast mutants defective in fatty acid synthetase and acetyl CoA carboxylase. *J. Cell Biol.* 134:949–961.

60. Gachet, Y., S. Tournier, …, J. S. Hyams. 2001. A MAP kinase-dependent actin checkpoint ensures proper spindle orientation in fission yeast. *Nature.* 412:352–355.

61. Tournier, S., Y. Gachet, …, J. B. A. Millar. 2004. Disruption of astral microtubule contact with the cell cortex activates a Bub1, Bub3, and Mad3-dependent checkpoint in fission yeast. *Mol. Biol. Cell.* 15:3345–3356.

62. Meadows, J. C., and J. Millar. 2008. Latrunculin A delays anaphase onset in fission yeast by disrupting an ase1-independent pathway controlling mitotic spindle stability. *Mol. Biol. Cell.* 19:3713–3723. https://www.molbiolcell.org/doi/10.1091/mbc.e08-02-0164.

63. Elting, M. W., C. L. Hueschen, …, S. Dumont. 2014. Force on spindle microtubule minus ends moves chromosomes. *J. Cell Biol.* 206:245–256. https://rupress.org/jcb/article/206/2/245/37798/Force-on-spindle-microtubule-minus-ends-moves.

64. Sikirzhytski, V., V. Magidson, …, A. Khodjakov. 2014. Direct kinetochore-spindle pole connections are not required for chromosome segregation. *J. Cell Biol.* 206:231–243.

65. Bratman, S. V., and F. Chang. 2007. Stabilization of overlapping microtubules by fission yeast CLASP. *Dev. Cell.* 13:812–827.

66. Gachet, Y., C. Reyes, …, S. Tournier. 2008. Sister kinetochore recapture in fission yeast occurs by two distinct mechanisms, both requiring Dam1 and Klp2. *Mol. Biol. Cell.* 19:1646–1662.

67. Tanenbaum, M. E., R. D. Vale, and R. J. McKenney. 2013. Cytoplasmic dynein crosslinks and slides anti-parallel microtubules using its two motor domains. *Elife.* 2013:1–20.

68. Hueschen, C. L., S. J. Kenny, …, S. Dumont. 2017. NuMA recruits dynein activity to microtubule minus-ends at mitosis. *Elife.* 6:1–26.

69. Burbank, K. S., T. J. Mitchison, and D. S. Fisher. 2007. Slide-and-cluster models for spindle assembly. *Curr. Biol.* 17:1373–1383.

70. Olmsted, Z. T., A. G. Colliver, …, J. L. Paluh. 2014. Kinesin-14 and kinesin-5 antagonistically regulate microtubule nucleation by γ-TuRC in yeast and human cells. *Nat. Commun.* 5:5339.